Acoustic scattering in waveguides that are discontinuous in geometry and material property

D P Warren, J B Lawrie[1] & I M Mohamed
Department of Mathematical Sciences
Brunel University
Uxbridge
Middlesex, UB8 3PH, U.K.
15*th* November 2001

The scattering of acoustic waves at the discontinuity between two ducts of different heights is considered. At least one of the ducts is bounded by a membrane and, thus, the underlying eigenproblem is *non-Sturm-Liouville*. A mode-matching procedure, based on an appropriate orthogonality relation, reduces the problem to that of truncating and solving an infinite system of linear equations. The distribution of power between the fluid regions and the membrane(s) is analysed. Further, it is shown that a fundamental property of the truncated system is that the expression for power balance is *always* satisfied.

1 Introduction

Structural acoustics is a field of engineering and applied mathematics that provides many challenging and interesting problems. The primary concern is usually the reduction of structural vibration and the noise associated with it. Such noise is generated by a variety of mechanisms but typically involves the scattering of waves at a discontinuity in either the material properties or the geometry of the object. For this reason it is important to understand the scattering characteristics of all the key features of a given structure. In fact, in the high frequency limit, the geometric theory of diffraction [1] enables the total sound field at any point in space to be calculated as the sum of all the scattered wave contributions. This alone justifies the study of a range of problems all of which are canonical to diffraction theory.

Problems that involve a change in the material properties of an otherwise planar structure may be amenable to solution by the Wiener-Hopf technique. Indeed, this has proven to be a powerful tool enabling the analytic solution of a variety of complicated problems involving the scattering of sound waves

[1]Corresponding author.

at an edge or sharp discontinuity. Classical articles in this vein include [2, 3, 4]. Alternatively, where the change in material property occurs in a less abrupt or smooth manner, a solution may be sought by modelling the material parameters as functions of the spatial variables. Although heuristic, such an approach may enable the boundary value problem to be recast as a difference equation, the solution to which provides valuable insight into the qualitative behaviour of the physical problem. This approach was originally formulated in [5] and has subsequently been employed in [6, 7, 8].

For structures that have a discontinuity in geometry, as opposed to material property, the above methods are inappropriate. One such class of problem comprises the scattering of sound in waveguides that have one or more abrupt changes in height. A change in geometry of this type may also coincide with a change in material property. A very simple example comprises a two-dimensional, semi-infinite duct with rigid surfaces which occupies the region $0 \leq y \leq a$, $x < 0$ of a non-dimenional Cartesian coordinate system (x, y) and is abutted onto a similar duct of height b, $b > a$ whose boundaries are soft (see figure 1). Given that the duct is closed by a finite vertical rigid surface occupying $x = 0$, $a \leq y \leq b$, then any incident wave propagating in the positive x direction will be scattered at the discontinuity into a potentially large number of reflected and transmitted waves. In fact, on assuming a harmonic time dependence of $e^{-i\omega t}$ where ω is the radian frequency, this particular problem can be solved in a fairly straightforward manner. After non-dimensionalising the boundary value problem with respect to length k^{-1} and time ω^{-1}, the time harmonic fluid velocity potential $\phi(x, y)$ may be expressed in terms of eigenfunctions expansions appropriate to the two duct regions. Thus,

$$\phi(x,y) = \begin{cases} e^{ix} + \phi_1(x,y), & x < 0, \quad 0 \leq y \leq a \\ \phi_2(x,y), & x > 0, \quad 0 \leq y \leq b \end{cases} . \tag{1}$$

where

$$\phi_1 = \frac{A_0}{2} e^{-ix} + \sum_{n=1}^{\infty} A_n \cos(\frac{n\pi y}{a}) e^{-i\eta_n x}, \qquad \eta_n = (1 - \frac{n^2\pi^2}{a^2})^{1/2} \tag{2}$$

and

$$\phi_2 = \sum_{n=0}^{\infty} B_n \cos(\frac{(2n+1)\pi}{2b} y) e^{i\nu_n x}, \qquad \nu_n = (1 - \frac{(2n+1)^2\pi^2}{4b^2})^{1/2} \quad . \tag{3}$$

Here the coeffcients A_n and B_n are the complex amplitudes of the n^{th} reflected and transmitted modes. Both of the above expansions are standard

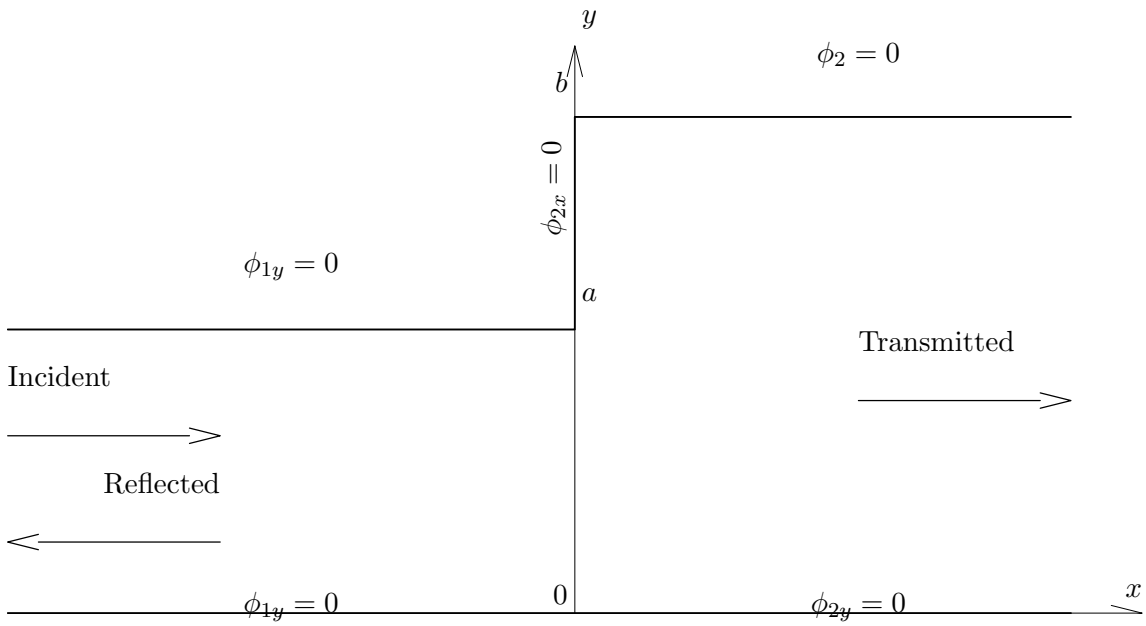

Figure 1: Physical configuration of the hard/soft problem. Note that $\phi_1(x, y)$ is the velocity potential corresponding to the reflected field and $\phi_2(x, y)$ corresponds to the transmitted field.

half-range Fourier cosine series and it follows that standard analysis will reduce the problem to an infinite system of linear algebraic equations which must then be solved for the coefficients A_n and B_n. The reader is referred to [9] for details of the method, it is sufficient here to quote the system as being

$$A_\ell = -2\delta_{0\ell} + \frac{2}{a}\sum_{m=0}^{\infty} B_m R_{\ell m} \tag{4}$$

where $\delta_{0\ell}$ is the usual Kronecker delta, together with

$$B_n = \frac{2}{\nu_n b}\left[\left(\frac{2 - A_0}{2}\right) R_{0n} - \sum_{\ell=1}^{\infty} \eta_\ell A_\ell R_{\ell n}\right] \tag{5}$$

where

$$R_{\ell m} = \frac{(-1)^{\ell+1}\frac{(2m+1)\pi}{2b}\sin\left(\frac{(2m+1)\pi a}{2b}\right)}{\frac{\ell^2\pi^2}{a^2} - \frac{(2m+1)^2\pi^2}{4b^2}}. \tag{6}$$

The problem summarized above is used as a reference model against which to compare the results that follow in the next two sections and it will,

henceforth, be refered to as the hard/soft problem. The method used to solve the hard/soft problem is a standard eigenfunction matching procedure and many examples of this process can be found in the literature, for example [10, 11]. Such an approach is, however, appropriate only for ducts whose surfaces are hard, soft or of Robin type (impedance) since, in these cases, separation of variables yields an eigen-problem of Sturm-Liouville type. For surfaces, such as membranes and elastic plates, that are described by high order boundary conditions the eigen-problems are not Sturm-Liouville. However, recent work in [9] and, for more general cases, in [12] has identified the orthogonality relations that are appropriate for this class of problem. This article is concerned with the application of one such orthogonality relation to two problems involving a waveguide that is discontinuous in height and in which at least one bounding surface comprises a membrane. Both problems are reduced to infinite systems of algebraic equations which are solved by truncation.

In §2.1 the scattering of a plane incident wave at the junction between a semi-infinite rigid duct and a semi-infinite membrane-bounded duct of different height is considered. It is convenient to refer to this problem as the hard/membrane problem (the name referring to the upper boundaries on either side of the height discontinuity). The preliminary numerical results of §2.2 are designed to confirm both the analytic integrity and the computational accuracy of the method developed herein. Thus, for the special case in which $a = b$, the results are compared with those obtained by recourse to the Wiener-Hopf technique whilst, for the situation $b > a$, the heavy fluid-loading limit is contrasted with the hard/soft problem summarized above. More general results are presented in the form of a comprehensive analysis of the distribution of power between the fluid regions and the membrane. These quantities are plotted against the non-dimensional height of the membrane bounded duct, b, (for fixed frequency) and against frequency (for fixed geometry and membrane parameters). The duct discussed in §3.1 has membrane boundaries on both sides of the height discontinuity and, for this reason, will be referred to as the membrane/membrane problem. The most general configuration, in which the two membranes have different material properties, is considered. In §3.2 the numerical results for a range of special cases are shown before progressing to more general results which again include a full analysis of the distribution of power in the system. A comprehensive discussion of the mode-matching method is presented in §4. It is shown that the mode-matching scheme conserves power regardless of the level to which the infinite system of equations is truncated. Finally, the Appendix contains derivations of the orthogonality relation, some supple-

mentary identities and a brief discussion of the power transmitted along a membrane bounded duct.

2 Reflection and transmission at the junction of a rigid duct with a membrane bounded duct of different height

The problem considered in this section is that of determining the sound field generated inside a wave-guide when a plane acoustic wave is scattered at a discontinuity in both height and material property. The wave-guide comprises two semi-infinite ducts of different heights, one with rigid surfaces and one with membrane boundaries (see figure 2). The solution method employs the standard procedure of separation of variables to express the fluid velocity potential in each duct region as an eigenfunction expansion. For the duct with rigid boundaries the eigenfunction expansion is a standard Fourier cosine series (see (2)). In contrast, due to the high order derivatives in the condition that describes the membrane boundary, the underlying eigensystem for the adjacent duct region is not Sturm-Liouville. However, application of the appropriate orthogonality relation (see Appendix) reduces the problem to an infinite system of linear equations which may be solved by truncation. As for the hard/soft problem discussed in §1, the boundary value problem is non-dimensionalized with respect to length k^{-1} and time ω^{-1}, where k is the fluid wavenumber and ω is the radian frequency of the time harmonic disturbances.

2.1 Statement and solution of the boundary value problem

The governing equation is Helmholtz's equation (the reduced wave equation), that is

$$\left\{\frac{\partial^2}{\partial x^2}+\frac{\partial^2}{\partial y^2}+1\right\}\phi=0, \tag{7}$$

in which $\phi(x,y)$ is the time harmonic, fluid velocity potential and x and y are Cartesian co-ordinates. Thus, the waveguide occupies the region $0\leq y\leq a$, $x<0$ and $0\leq\ y\leq b$, $x>0$, with $b\geq a>0$, and is closed so that the vertical surface $x=0$, $a<y<b$ forms part of its boundary. The surface $y=b$, $x>0$ comprises a membrane whilst every other surface is acoustically hard (see figure 2).

The interior region of the waveguide contains a compressible fluid whilst the exterior is *in vacuo*. It is convenient to divide the fluid velocity potential

into two parts such that

$$\phi = \begin{cases} e^{ix} + \phi_1, & x < 0 \\ \phi_2, & x > 0 \end{cases} . \tag{8}$$

Thus, the boundary conditions at the horizontal rigid surfaces can be expressed as

$$\frac{\partial \phi_j}{\partial y} = 0, \qquad y = 0, \quad -\infty < x < \infty, \quad j = 1, 2 , \tag{9}$$

$$\frac{\partial \phi_1}{\partial y} = 0, \qquad y = a, \quad x < 0. \tag{10}$$

The bounding membrane surface satisfies condition (A.77), that is

$$\left\{ \frac{\partial^2}{\partial x^2} + \mu^2 \right\} \phi_{2y} + \alpha \phi_2 = 0, \qquad y = b, \quad x = 0 \tag{11}$$

where the non-dimensional parameters μ and α are defined in (A.78). At the matching interface $x = 0$, the fluid pressure and the normal component of velocity are continuous in the fluid whilst the latter vanishes at the vertical rigid surface. That is

$$1 + \phi_1 = \phi_2, \qquad x = 0, \quad 0 \le y \le a, \tag{12}$$

$$\frac{\partial \phi_2}{\partial x} = \begin{cases} 0, & x = 0, \quad a < y \le b \\ i + \frac{\partial \phi_1}{\partial x}, & x = 0, \quad 0 \le y \le a \end{cases} . \tag{13}$$

At the point where the membrane surface meets the rigid vertical surface (i.e. at $x = 0$, $y = b$) an edge condition must be imposed. The choice of edge condition can significantly affect the scattered field and there are two options, either

$$\phi_{2y}(0, b) = 0, \tag{14}$$

$$\text{or} \qquad \phi_{2xy}(0, b) = 0. \tag{15}$$

The first condition is consistent with the membrane being tethered at the point $(0, b)$ but with unspecified gradient. The second condition, implies that the membrane may slide in the vertical plane provided it has zero gradient.

The scattered potential, $\phi_1(x, y)$, comprises an infinite sum of reflected waves, each of which must satisfy conditions (9) and (10) whilst being a solution of (7). Thus,

$$\phi_1 = \frac{A_0}{2} e^{-ix} + \sum_{n=1}^{\infty} A_n \cos\left(\frac{n\pi y}{a}\right) e^{-i\eta_n x} \tag{16}$$

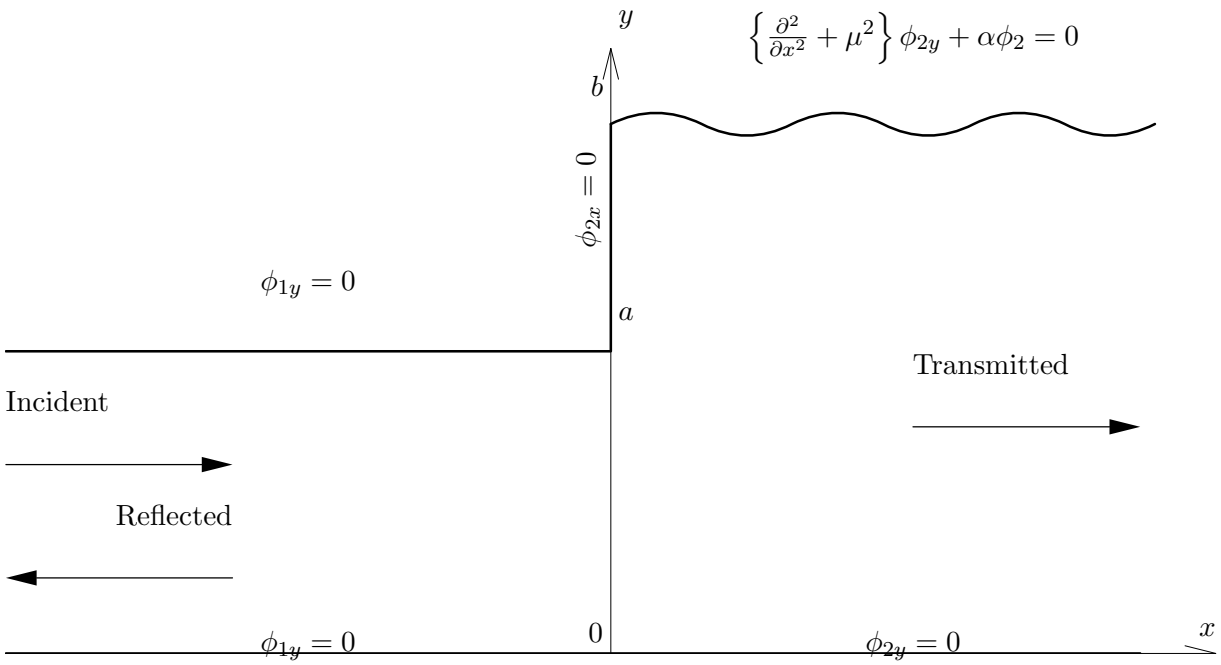

Figure 2: Physical configuration of the hard/membrane problem.

where $A_n, n = 0, 1, 2, \ldots$ are the complex amplitudes of each mode, and $\eta_n = (1 - n^2\pi^2/a^2)^{1/2}$. The duct occupying the region $x > 0$ is of exactly the same form as that discussed in the Appendix and it follows that

$$\phi_2 = \sum_{n=0}^{\infty} B_n \cosh(\gamma_n y)\, e^{i\nu_n x} \tag{17}$$

where $s = \pm\nu_n = \pm(1 + \gamma_n^2)^{\frac{1}{2}}$, $n = 0, 1, 2, \ldots$ are the roots of the dispersion relation which, for convenience, is defined in terms of the variable s and the duct height b as

$$K(s, b) = (s^2 - \mu^2)\gamma \sinh(\gamma b) - \alpha \cosh(\gamma b) = 0, \quad \gamma = (s^2 - 1)^{1/2}. \tag{18}$$

The complex amplitudes, A_n and B_n of equations (16) and (17) are, as yet undetermined and are to be found by appealing to continuity of pressure and normal velocity, that is (12) and (13). From (12) it is found that

$$\frac{2 + A_0}{2} + \sum_{\ell=1}^{\infty} A_\ell \cos\left(\frac{\ell\pi y}{a}\right) = \sum_{m=0}^{\infty} B_m \cosh(\gamma_m y)\,. \tag{19}$$

Application of standard Fourier analysis to the left hand side of (19) shows the coefficients $A_\ell, \ell = 0, \ldots, \infty$ to be given by

$$A_\ell = -2\delta_{0\ell} + \frac{2}{a}\sum_{m=0}^{\infty} B_m R_{\ell m} \tag{20}$$

where $\delta_{0\ell}$ is the Kronecker delta and

$$R_{\ell m} = \int_0^a \cos\left(\frac{\ell\pi y}{a}\right)\cosh(\gamma_m y)dy = \frac{(-1)^\ell \sinh(\gamma_m a)}{\left(1+\frac{\ell^2\pi^2}{\gamma_m^2 a^2}\right)\gamma_m}. \tag{21}$$

Similar expressions for $B_n, n = 0, \ldots, \infty$ are required and are found by recourse to (13) which may be rewritten as

$$\phi_{2x}(0,y) = \begin{cases} 0, & a \le y \le b \\ i\left(\frac{2-A_0}{2}\right) - \sum_{\ell=1}^{\infty} i\eta_\ell A_\ell \cos\left(\frac{\ell\pi y}{a}\right), & 0 \le y < a \end{cases}. \tag{22}$$

On recalling that the eigenfunction expansion of $\phi_2(0,y)$ is given by (17), the inner product defined in (A.91) is used to obtain

$$\alpha\int_0^b \phi_{2x}(0,y)\cosh(\gamma_n y)dy + \gamma_n \sinh(\gamma_n b)E = iB_n\nu_n C_n, \quad n = 0,1,2,\ldots, \tag{23}$$

where C_n is given by (A.88) but may be recast as

$$C_n = \frac{\alpha b}{2} + \left(\gamma_n^2 + \frac{\nu_n^2 - \mu^2}{2}\right)\sinh^2(\gamma_n b), \tag{24}$$

and

$$E = \phi_{2xy}(0,b) = i\sum_{m=0}^{\infty} B_m\nu_m\gamma_m \sinh(\gamma_m b). \tag{25}$$

Then, on using (22), it is found that

$$iB_n\nu_n C_n = \gamma_n \sinh(\gamma_n b)E + \alpha i\int_0^a \left[\frac{2-A_0}{2} - \sum_{\ell=1}^{\infty}\eta_\ell A_\ell \cos\left(\frac{\ell\pi y}{a}\right)\right]\cosh(\gamma_n y)\, dy, \tag{26}$$

which reduces to

$$B_n = \frac{-i\gamma_n \sinh(\gamma_n b)E}{\nu_n C_n} + \frac{\alpha}{\nu_n C_n}\left[\frac{(2-A_0)R_{0n}}{2} - \sum_{\ell=1}^{\infty}\eta_\ell A_\ell R_{\ell n}\right], \quad n = 0,1,2,\ldots. \tag{27}$$

On eliminating A_ℓ between (20) and (27), the following infinite system of equations is obtained

$$\begin{aligned} B_n &= \frac{-i\gamma_n \sinh(\gamma_n b)E}{\nu_n C_n} \\ &+ \frac{2\alpha}{\nu_n C_n}\left[R_{0n} - \frac{R_{0n}}{2a}\sum_{m=0}^{\infty} B_m R_{0m} - \frac{1}{a}\sum_{\ell=1}^{\infty}\sum_{m=0}^{\infty} B_m \eta_\ell R_{\ell m} R_{\ell n}\right]. \end{aligned} \tag{28}$$

It is clear that the system is indeterminate since truncation of the system at, say, $n = N$ will provide only N equations by which to determine $N + 1$ coefficients, that is, E and B_n, $n = 1, 2, 3 \ldots, N$. A further equation is obtained by application of either edge condition (14) or (15).

It is straightforward to impose condition (15), in this case $E = 0$ by definition (see (25)). To enforce edge condition, (14), is also relatively simple. On differentiating (17) with respect to y and substituting for B_n using (28), it is found that

$$iE = \frac{\alpha \displaystyle\sum_{n=0}^{\infty} \frac{\gamma_n \sinh(\gamma_n b)}{\nu_n C_n}\left[2R_{0n} - \frac{R_{0n}}{a}\sum_{m=0}^{\infty} B_m R_{0m} - \frac{2}{a}\sum_{l=1}^{\infty}\sum_{m=0}^{\infty} B_m \eta_l R_{lm} R_{ln}\right]}{\displaystyle\sum_{j=0}^{\infty} \frac{\gamma_j^2 \sinh^2(\gamma_j b)}{\nu_j C_j}}. \tag{29}$$

The system of linear algebraic equations defined by (28) together with either E=0 or (29) is suitably convergent. Thus, the solution to the physical problem is obtained by truncating at, say, N equations and solving the reduced system. Results are presented in §2.2 below.

2.2 Numerical Results

For the special case in which $a = b$, the problem can be solved by means of the Wiener-Hopf technique and this provides an excellent check for the method employed herein. For brevity the Wiener-Hopf analysis is omitted here but can be found in [9]. The reader is also refered to [2, 3] where the technique is applied to problems involving the scattering of fluid-coupled plate waves at an edge or junction. When the edge condition $\phi_y(0, b) = 0$ is applied, the modulus of the reflection coefficient of the fundamental mode is found to be

$$|R| = \frac{\alpha}{4a|K_+(1)|^2}, \tag{30}$$

where $K_+(s)$ is defined by

$$K(s) = K_+(s)K_-(s) = (s^2 - \mu^2) - \frac{\alpha \cosh(\gamma a)}{\gamma \sinh(\gamma a)}, \quad \gamma = (s^2 - 1)^{1/2} \qquad (31)$$

such that $K_\pm(s)$ is analytic and non-zero in the upper/lower half of the complex s-plane. Note that, $K(s)$ is the Wiener-Hopf kernel for this problem and is essentially the dispersion function given by (18) with b replaced by a.

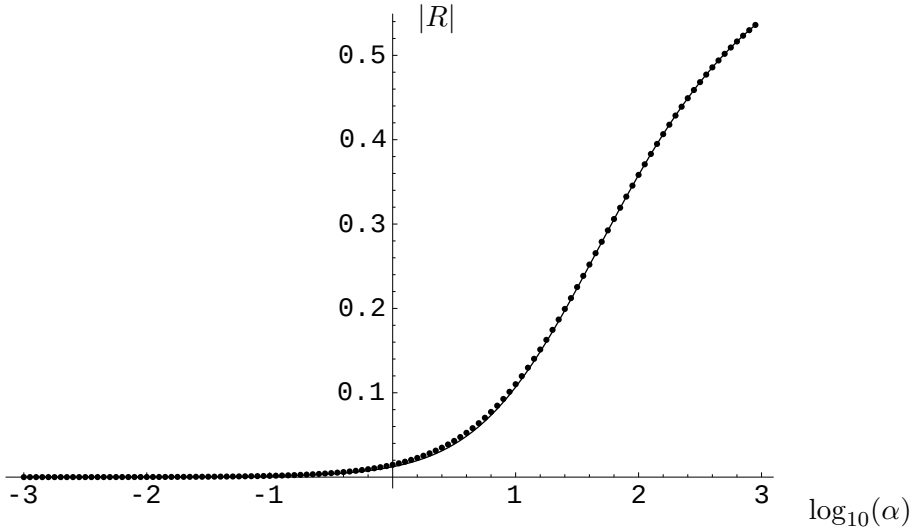

Figure 3: Comparison of the modulus of the reflection coefficient of the fundamental mode for the hard/membrane problem (solid line) and Wiener-Hopf solution (dots) with edge condition: $\phi_y(0, b) = 0$; ($a = b = 1$; $\mu = 2.2$).

Figure 3 shows the modulus of the reflection coefficient of the fundamental mode plotted against $\log_{10}(\alpha)$ for $a = b = 1$ and $\mu = 2.2$ with the zero displacement edge condition. The solid line is the value for $|A_0|/2$ obtained by solving the truncated system (28) together with (29) whilst the dots are the corresponding values given by (30). There is clearly exact agreement

between the two sets of data.

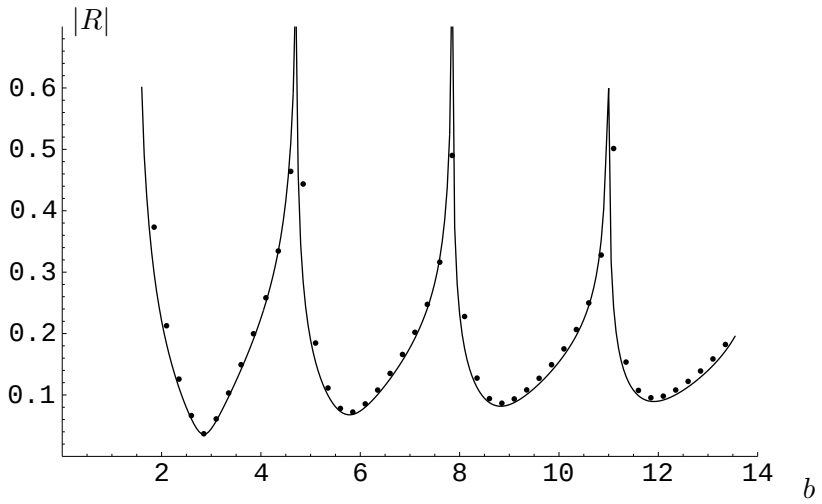

Figure 4: Comparison of the modulus of the reflection coefficient of the fundamental mode for the hard/membrane problem (solid line) with that for the hard/soft problem (dots), ($a = 1.6$, $\alpha = 5000$, $\mu = 2.2$).

A further check on the analysis, this time for the general geometry $b \geq a$, is obtained by considering the large α limiting behaviour of the membrane lying along $y = b$, $x > 0$. In this, the heavy fluid-loading limit, the membrane boundary condition is approximated by $\phi(x, b) = 0$, $x > 0$ which represents a significant simplification. Thus, a suitable comparision problem is that in which the membrane is replaced by a soft boundary, that is, the hard/soft problem discussed in §1. In order for the membrane behaviour to mimic the soft wall condition, α must be large, say $\alpha \geq 500$, and μ must be small in comparison, ideally $O(1)$. Figure 4 is a graph of the modulus of the reflection coefficient (that is, $R = A_0/2$) obtained by truncation of (28) (in this case the choice of edge condition is immaterial) with that obtained from (4) – (6). There is excellent agreement between the two sets of results. Note that this figure demonstrates behaviour that is characteristic to the reflection coefficient. That is, it peaks every time b increases suffiently for a new transmitted mode to be switched on: in this case at $b = (n + 1/2)\pi$, $n = 0, 1, 2, \ldots$.

The results presented above are designed to demonstrate the effectiveness of the mode-matching technique presented in this article by comparing

limiting cases with known solutions. The next two graphs show the distribution of power between the two fluid regions and the membrane. Expression (A.101) is easily used to obtain the power reflected along the rigid duct of height a, whilst the power transmitted in the membrane bounded duct is (after minor modification to the notation) given by (A.105). Hence, the power balance is given by

$$1 \equiv \Re\left\{\sum_{n=0}^{\infty}\left[\frac{|A_n|^2\eta_n}{2\epsilon_n} + \frac{|B_n|^2\nu_n}{a}\left(\frac{b}{2} + \frac{\sinh(2\gamma_n b)}{4\gamma_n}\right) + \frac{|B|^2\nu_n}{\alpha a}\gamma_n^2\sinh(2\gamma_n b)\right]\right\} \tag{32}$$

where $\epsilon_0 = 2$ and $\epsilon_n = 1$, $n \geq 1$. The first two quantities on the right hand side of (32) correspond to the reflected and transmitted power in the two separate fluid regions, whilst the third term is the power flux along the membrane. These three terms are plotted in figures 5 and 6 for a membrane of mass 2/3 kg per unit area and with tension 2000 N per metre in the z direction. The density of air is taken as 1.2043 kg m^{-3} and the sound speed in air as 343.5 ms^{-1}.

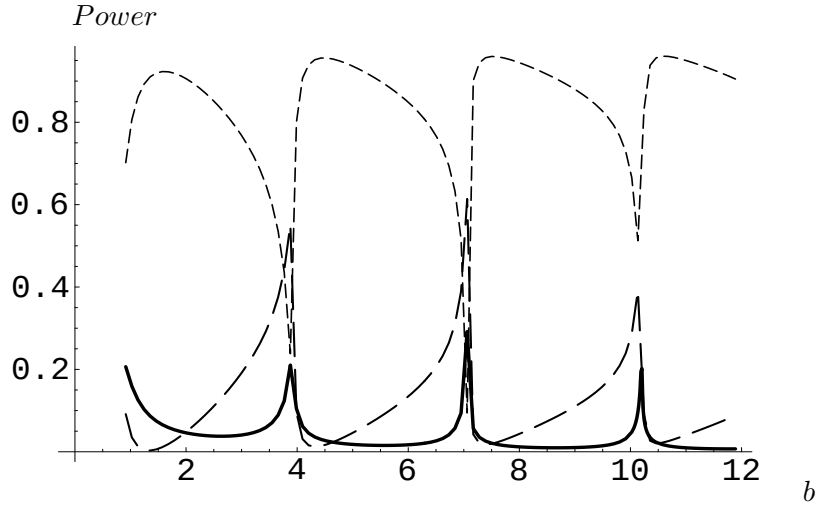

Figure 5: Distribution of power between the two fluid regions and the membrane as the membrane bounded duct height varies: *short dash* ≡ transmitted; *long bold dash* ≡ reflected; *solid line* ≡ membrane. (Frequency is 100 Hz and $a = 0.915$, $\alpha = 38.84$, $\mu = 9.41$.)

Figure 5 shows the distribution of power for forcing frequency of 100 Hz, thus $k = 1.83$. The physical height of the rigid duct is 0.5m (the non-dimensional equivalent is $a = 0.915$) whilst the physical height of the

membrane bounded duct varies from $0.5 - 6.5$m (i.e., b varies from 1.83 to 11.9). In this case $\mu = 9.41$ and $\alpha = 38.84$. It is clear that, overall, most of the power is transmitted in the fluid region of the membrane bounded duct. However, the sudden troughs in this curve correspond to the values of b for which another fluid-membrane coupled mode is *cut-on*. In contrast the reflected power, which is generally smaller, peaks whenever the transmitted power troughs (c.f. figure 4). The membrane transmits significantly less power but, perhaps surprisingly, this also peaks as a new fluid-membrane mode is *cut-on*.

Figure 6 shows the distribution of power for fixed geometry and membrane parameters as the forcing frequency increases from $5 - 650$ Hz. In this case the height of the rigid duct is 0.5m whilst that of the membrane bounded duct is 0.8m. As in the previous figure, the transmitted power drops as a new transmitted mode is cut-on whilst the reflected and membrane powers peak. There is a small peak in the transmitted power at approximately 343 Hz, this corresponds to a new reflected mode being cut-on. For very low frequencies (less than 100 Hz) the membrane transmits a significant proportion of the power, but this rapidly tends to zero as the frequency increases. In fact, for frequencies greater that 650 Hz well over 95% of the power is transmitted through the fluid region of the membrane bounded duct whilst the remainder is reflected.

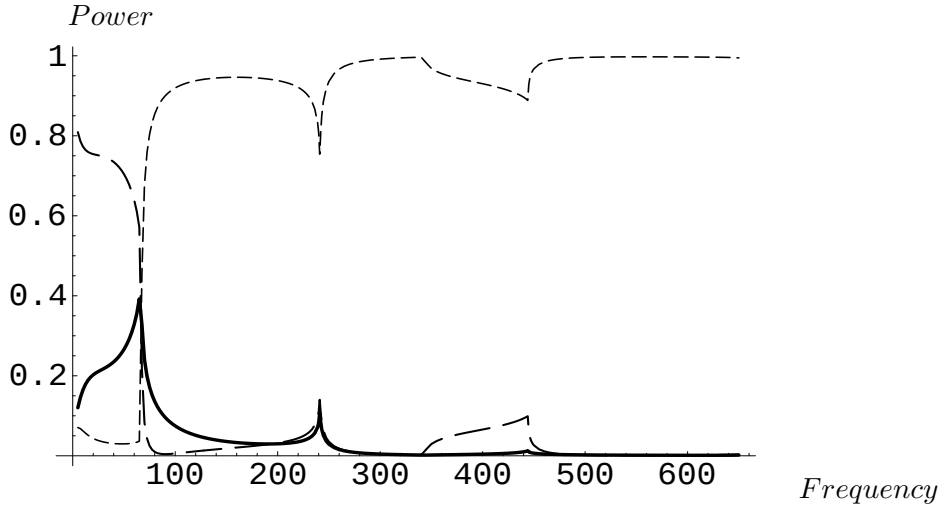

Figure 6: Distribution of power between the two fluid regions and the membrane as frequency varies: *short dash* $\equiv$ transmitted; *long bold dash* $\equiv$ reflected; *solid line* $\equiv$ membrane. (Here $a/b = 5/8$ and $\mu = 9.41$.)

3 Reflection and transmission at the junction of two membrane bounded ducts of different heights and material properties

The problem considered here differs from that of §2 in that the left hand duct also has membrane boundaries but with different material properties from those on the right hand side (see figure 7). The analysis is more complicated since the eigen-system for neither duct region is Sturm-Liouville in type, the orthogonality relation (A.91) must be applied twice and there are now four sets of edge conditions to consider. For convenience, this problem is referred to as the membrane/membrane problem.

3.1 Statement and solution of the boundary value problem

As before, the two dimensional wave-guide occupies the region $0 \leq y \leq a$, $x < 0$ and $0 \leq y \leq b$, $x > 0$ with $b > a$ and is closed so that the vertical surface $x = 0$, $a \leq y \leq b$ forms part of its boundary. In this case, however, only the infinite surface lying along $y = 0$ and the finite vertical surface are rigid. The remaining surfaces comprise two membranes, with different material properties, occupying $y = a$, $x < 0$ and $y = b$, $x > 0$ respectively (see figure 7). Forcing is introduced in the form of a fluid-coupled structural wave which propagates in the positive x-direction towards $x = 0$.

It is convenient to express the fluid velocity potential in terms of the forcing term and two scattered potentials. Thus,

$$\phi = \begin{cases} \frac{\cosh(\tau_0 y)}{\cosh(\tau_0 a)} e^{i\eta_0 x} + \phi_1, & x < 0 \\ \phi_2, & x > 0 \end{cases}, \tag{33}$$

where $\tau_0 = (\eta_0^2 - 1)^{\frac{1}{2}}$ and η_0 is the wavenumber of the fluid-coupled structural wave for the membrane lying along $y = a$, $x < 0$, see (45). As usual, the governing equation is Helmholtz's equation

$$\left\{ \frac{\partial^2}{\partial x^2} + \frac{\partial^2}{\partial y^2} + 1 \right\} \phi = 0, \tag{34}$$

and for brevity the boundary conditions are simply stated as

$$\frac{\partial \phi_j}{\partial y} = 0, \qquad y = 0, \quad -\infty < x < \infty, \quad j = 1, 2 \tag{35}$$

$$\left\{ \frac{\partial^2}{\partial x^2} + \mu_1^2 \right\} \phi_{1y} + \alpha_1 \phi_1 = 0, \qquad y = a, \quad x < 0, \tag{36}$$

$$\left\{\frac{\partial^2}{\partial x^2}+\mu_2^2\right\}\phi_{2y}+\alpha_2\phi_2 \;=\; 0, \qquad y=b, \quad x>0. \tag{37}$$

At the matching interface, continuity of pressure and normal velocity give

$$\frac{\cosh(\tau_0 y)}{\cosh(\tau_0 a)}+\phi_1=\phi_2, \qquad\qquad x=0, \quad 0\le y\le a, \tag{38}$$

and

$$\frac{\partial\phi_2}{\partial x}=\begin{cases} 0, & x=0, \quad a<y\le b \\ \frac{\partial\phi_1}{\partial x}+\frac{i\eta_0\cosh(\tau_0 y)}{\cosh(\tau_0 a)}, & x=0, \quad 0\le y\le a \end{cases}. \tag{39}$$

As before it is necessary to enforce either zero membrane displacement or zero gradient at the the points $x=0$, $y=a$ and $x=0$, $y=b$ (where the two membranes meet the finite vertical rigid barrier). That is, either

$$\tau_0\tanh(\tau_0 a)+\phi_{1y}(0,a) \;=\; 0, \tag{40}$$

$$\text{or} \qquad i\eta_0\tau_0\tanh(\tau_0 a)+\phi_{1xy}(0,a) \;=\; 0, \tag{41}$$

for the left hand membrane, and either

$$\phi_{2y}(0,b) \;=\; 0, \tag{42}$$

$$\text{or} \qquad \phi_{2xy}(0,b) \;=\; 0. \tag{43}$$

for the right hand membrane (see 14 and 15). There are four possible combinations of these conditions and each will be considered.

The eigenfunction expansions for the potentials $\phi_1(x,y)$ and $\phi_2(x,y)$ are analogous to those of §2. Thus, it is sufficient to state

$$\phi_1=\sum_{n=0}^{\infty}A_n\cosh(\tau_n y)e^{-i\eta_n x} \tag{44}$$

where $s=\pm\eta_n, n=0,1,2,\ldots$ are the roots of

$$K_1(s,a)=(s^2-\mu_1^2)\gamma\sinh(\gamma a)-\alpha_1\cosh(\gamma a)=0, \quad \gamma=(s^2-1)^{1/2} \tag{45}$$

whilst

$$\phi_2=\sum_{n=0}^{\infty}B_n\cosh\left(\gamma_n y\right)e^{i\nu_n x} \tag{46}$$

where $s=\pm\nu_n$, $n=0,1,2,\ldots$ are the roots of the dispersion relation

$$K_2(s,b)=(s^2-\mu_2^2)\gamma\sinh(\gamma b)-\alpha_2\cosh(\gamma b)=0, \quad \gamma=(s^2-1)^{1/2}. \tag{47}$$

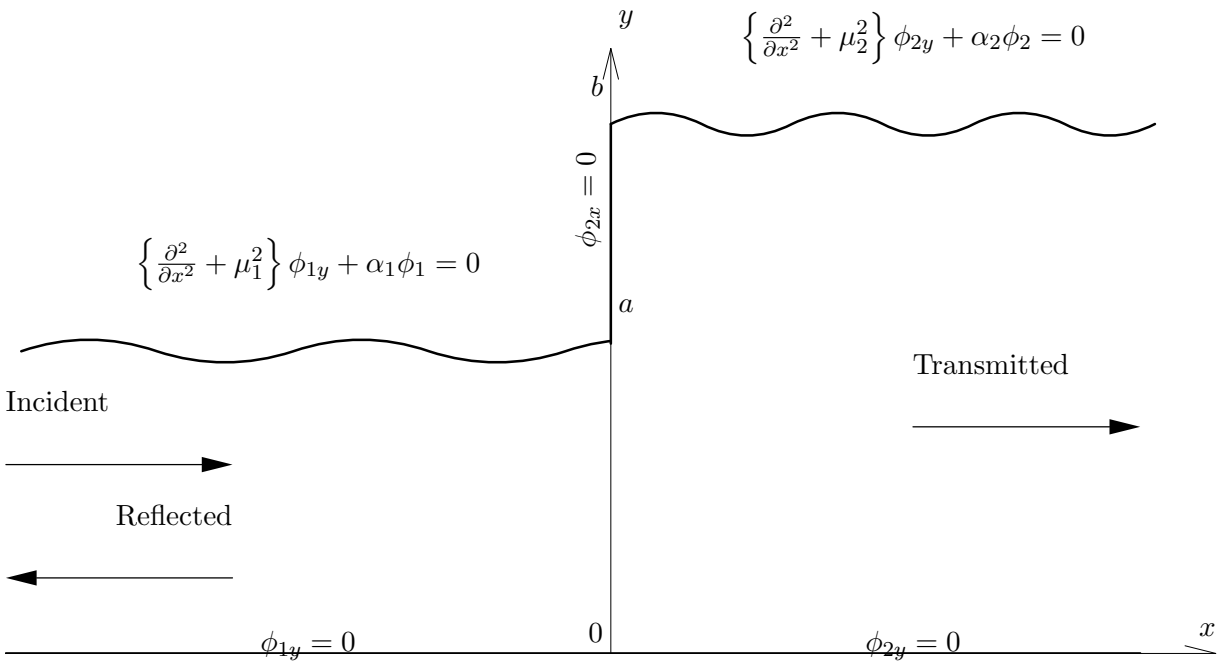

Figure 7: Physical Configuration for the membrane/membrane problem.

Henceforth the notation $\gamma(\eta_n) = \tau_n$ and $\gamma(\nu_n) = \gamma_n$ is adopted to denote the wavenumber components in the y-direction of $\phi_1(x, y)$ and $\phi_2(x, y)$ respectively.

The complex amplitudes, A_n and B_n, of equations (44) and (46) are to be determined, and the first step is to apply the matching conditions (38) and (39). From (38) it is found that

$$\phi_1(0, y) = -\frac{\cosh(\tau_0 y)}{\cosh(\tau_0 a)} + \sum_{m=0}^{\infty} B_m \cosh(\gamma_m y). \tag{48}$$

The inner product defined in (A.91) is now used to obtain

$$\alpha_1 \int_0^a \phi_1(0, y) \cosh(\tau_\ell y)\, dy + \tau_\ell \sinh(\tau_\ell a)\,[F - \tau_0 \tanh(\tau_0 a)] = A_\ell D_\ell \tag{49}$$

where

$$D_\ell = \frac{\alpha_1 a}{2} + \left(\tau_\ell^2 + \frac{\eta_\ell^2 - \mu_1^2}{2}\right) \sinh^2(\tau_\ell a), \tag{50}$$

and

$$F = \sum_{n=0}^{\infty} B_n \gamma_n \sinh(\gamma_n y). \tag{51}$$

On rearranging this and using (48) it is found that

$$\begin{aligned} A_\ell D_\ell &= \tau_\ell \sinh(\tau_\ell a)\left[F - \tau_0 \tanh(\tau_0 a)\right] \\ &+ \alpha_1 \int_0^a \left[\sum_{m=0}^{\infty} B_m \cosh(\gamma_m y) - \frac{\cosh(\tau_0 y)}{\cosh(\tau_0 a)}\right] \cosh(\tau_\ell y)\, dy, \end{aligned} \tag{52}$$

which reduces to

$$A_\ell = \frac{\alpha_1}{D_\ell} \sum_{m=0}^{\infty} B_m T_{\ell m} + \frac{\tau_\ell \sinh(\tau_\ell a) F}{D_\ell} - \frac{\delta_{0\ell}}{\cosh(\tau_0 a)}, \quad \ell = 0, 1, 2, \ldots \tag{53}$$

where

$$\begin{aligned} T_{\ell m} &= \int_0^a \cosh(\tau_\ell y) \cosh(\gamma_m y)\, dy \\ &= \frac{\tau_\ell \sinh(\tau_\ell a)\cosh(\gamma_m a) - \gamma_m \sinh(\gamma_m a)\cosh(\tau_\ell a)}{\tau_\ell^2 - \gamma_m^2}. \end{aligned} \tag{54}$$

To obtain a similar expressions for $B_n, n = 0, 1, 2, \ldots$, boundary condition (39) is rewritten as

$$\phi_{2x}(0, y) = \begin{cases} 0, & a \le y \le b \\ -\displaystyle\sum_{\ell=0}^{\infty} i\eta_\ell A_\ell \cosh(\tau_\ell y) + \frac{i\eta_0 \cosh(\tau_0 y)}{\cosh(\tau_0 a)}, & 0 \le y < a \end{cases}. \tag{55}$$

Once again the inner product is used to obtain

$$\alpha_2 \int_0^b \phi_{2x}(0, y) \cosh(\gamma_n y)\, dy + \gamma_n \sinh(\gamma_n b) E = i B_n \nu_n C_n, \quad n = 0, 1, 2, \ldots, \tag{56}$$

where

$$C_n = \frac{\alpha_2 b}{2} + \left(\gamma_n^2 + \frac{\nu_n^2 - \mu_2^2}{2}\right) \sinh^2(\gamma_n b), \tag{57}$$

and

$$E = \phi_{2xy}(0, b) = i \sum_{m=0}^{\infty} B_m \nu_m Y_{2m}^{'}(b). \tag{58}$$

This may be rearranged as

$$B_n = \frac{-i\gamma_n \sinh(\gamma_n b) E}{\nu_n C_n} + \frac{\alpha_2}{\nu_n C_n}\left[\frac{\eta_0 T_{0n}}{\cosh(\tau_0 a)} - \sum_{\ell=0}^{\infty} \eta_\ell A_\ell T_{\ell n}\right], \quad n = 0, 1, 2, \ldots \quad . \tag{59}$$

Equations (53) and (59) comprise a pair of coupled infinite systems for A_n and B_n. On eliminating A_n between these it is found that

$$B_n = \frac{-i\gamma_n \sinh(\gamma_n b)E}{\nu_n C_n} + \frac{\alpha_2}{\nu_n C_n}\left[\frac{2\eta_0 T_{0n}}{\cosh(\tau_0 a)} - \sum_{\ell=0}^{\infty}\frac{\eta_\ell T_{\ell n}\tau_\ell \sinh(\tau_\ell a)F}{D_\ell}\right. \\ \left. - \alpha_1 \sum_{\ell=0}^{\infty}\sum_{m=0}^{\infty}\frac{\eta_\ell B_m T_{\ell m} T_{\ell n}}{D_\ell}\right]. \quad (60)$$

Expression (60) is an infinite system of linear algebraic equations from which the coefficients B_n may be determined. However, before the system can be solved it is necessary to specify the constants E and F. These are determined via the edge conditions (40)–(43). The four possible cases are summarised below.

Case (i): $\tau_0 \tanh(\tau_0 a) + \phi_{1y}(0,a) = \phi_{2y}(0,b) = 0$**.**
This corresponds to zero membrane displacement at both edges. On differentiating (46) with respect to y and substituting for B_n using (60), it is easily shown that

$$E = \frac{-i\alpha_2 \sum_{n=0}^{\infty}\frac{\gamma_n \sinh(\gamma_n b)}{\nu_n C_n}\left[\frac{2\eta_0 T_{0n}}{\cosh(\tau_0 a)} - \alpha_1 \sum_{\ell=0}^{\infty}\sum_{m=0}^{\infty}\frac{\eta_\ell B_m T_{\ell m} T_{\ell n}}{D_\ell}\right]}{\sum_{j=0}^{\infty}\frac{\gamma_j^2 \sinh^2(\gamma_j b)}{\nu_j C_j}}. \quad (61)$$

Likewise, on using (44) and (53), it is found that

$$F = \frac{-\alpha_1 \sum_{m=0}^{\infty} B_m \sum_{\ell=0}^{\infty}\frac{\tau_\ell \sinh(\tau_\ell a) T_{\ell m}}{D_\ell}}{\sum_{j=0}^{\infty}\frac{\tau_j^2 \sinh^2(\tau_j a)}{D_j}} \quad (62)$$

which reduces to $F = 0$ via (A.94) and (A.95).

Case (ii): $i\eta_0\tau_0 \tanh(\tau_0 a) + \phi_{1xy}(0,a) = \phi_{2y}(0,b) = 0$**.**
Here the right hand membrane has zero displacement at the edge $x = 0$, $y = b$ whereas the left hand membrane is specified to have zero gradient at

$x = 0$, $y = a$. In this case,

$$F = \frac{2\eta_0\tau_0 \tanh(\tau_0 a) - \alpha_1 \displaystyle\sum_{\ell=0}^{\infty}\sum_{m=0}^{\infty} \frac{\eta_\ell \tau_\ell B_m T_{\ell m} \sinh(\tau_\ell a)}{D_\ell}}{\displaystyle\sum_{j=0}^{\infty} \frac{\eta_j \tau_j^2 \sinh^2(\tau_j a)}{D_j}}, \tag{63}$$

and E is given by (61).

Case (iii): $\tau_0 \tanh(\tau_0 a) + \phi_{1y}(0, a) = \phi_{2xy}(0, b) = 0$**.**
This is the reverse of case (ii), that is, the left hand membrane has zero displacement and the right hand one has zero gradient. It is found that, $E = 0$ and $F = 0$.

Case (iv): $i\eta_0\tau_0 \tanh(\tau_0 a) + \phi_{1xy}(0, a) = \phi_{2xy}(0, b) = 0$**.**
In this case, both membrane have unspecified displacement but zero gradient at their respective edges. For this combination of edge conditions $E = 0$ and F is given by (63).

Equation (60) together with one set of edge conditions form a highly convergent system which can be truncated and solved numerically. Results for the edge conditions specified by cases (i) and (iv) are presented below.

3.2 Numerical Results

The Wiener-Hopf technique can be used to solve the above problem for the special case $a = b$. Only the relevant results are quoted here and the reader is refered to [9] for detail. Further, although there are four possible sets of edge conditions only cases (i) and (iv) will be considered.

For case (i) (i.e. zero displacement at both membrane edges), the Wiener-Hopf technique gives the modulus of the reflection coefficient of the fluid-coupled structural wave to be

$$|R| = \left| \frac{[K_+(\eta_0)]^2 K_2(\eta_0)}{K_1'(\eta_0)} \left[\frac{1}{2\eta_0} - \frac{1}{\eta_0 - \sigma} + \frac{2\sigma K_+(\sigma)}{[K_+(\sigma) - K_-(\sigma)](\eta_0^2 - \sigma^2)} \right] \right| \tag{64}$$

where

$$\sigma = \frac{\alpha_2\mu_1^2 - \alpha_1\mu_2^2}{\alpha_2 - \alpha_1} \tag{65}$$

and the Wiener-Hopf kernel is defined by

$$K(s) = K_+(s)K_-(s) = \frac{K_1(s,a)}{K_2(s,a)} = \frac{(s^2-\mu_1^2)\gamma\sinh(\gamma a) - \alpha_1\cosh(\gamma a)}{(s^2-\mu_2^2)\gamma\sinh(\gamma a) - \alpha_2\cosh(\gamma a)} \tag{66}$$

with $\gamma = (s^2-1)^{1/2}$. As usual, the product factors $K_\pm(s)$ are analytic and non-zero in the upper/lower half of the complex s-plane.

For case (iv) (i.e. zero gradient at both membrane edges), the Wiener-Hopf technique yields the following expression

$$|R| = \left| \frac{[K_+(\eta_0)]^2 K_2(\eta_0)}{K_1'(\eta_0)} \left[\frac{1}{2\eta_0} - \frac{(\Lambda-\eta_0)[K_+(\sigma)(\eta_0-\sigma) + K_-(\sigma)(\eta_0+\sigma)]}{(\eta_0^2-\sigma^2)[K_+(\sigma)(\Lambda-\sigma) + K_-(\sigma)(\Lambda+\sigma)]} \right] \right| \tag{67}$$

where $\Lambda = I_1 - I_2$ and

$$I_j = \mu_j + \frac{i}{\pi}\int_0^\infty \log\left\{1 - \frac{\alpha_j\coth(\gamma a)}{\gamma(\zeta^2-\mu_j^2)}\right\} d\zeta, \quad j = 1,2. \tag{68}$$

Here $\gamma = (\zeta^2-1)^{\frac{1}{2}}$ and the path of integration passes below any singularities on the real axis.

In figure 8 results for the Wiener-Hopf method are compared with those obtained by truncating the infinite system of linear algebraic equations derived above. The graph shows the modulus of the reflected wave (that is, (64) for the Wiener-Hopf technique and A_0 for the eigenfunction expansion method) against $\log_{10}(\alpha_1)$ using the edge conditions specified as case (i). It is remarkable that, even for a very severe truncation (10 equations), the agreement between the two methods is excellent up until $\alpha_1 \approx 750$. The loss of accuracy in the mode-matching method for $\alpha_1 > 750$ is attributed to behaviour of the roots of the dispersion relation. This is illustrated by expanding $\tau_n = (\eta_n^2-1)^{1/2}$, where η_n is a root of $K_1(s,a)$, asymptotically for large n. It is easily shown that

$$\tau_n \approx \frac{in\pi}{a} + \frac{i\alpha_1 a^2}{n^3\pi^3} + O(n^{-4}), \quad n >> 1, \tag{69}$$

and it is clear that, when α_1 is of the same order as n^3 the second term of this expansion becomes significant and so that the first term is then a poor approximation to τ_n. Analogously, the numerical error obtained in truncating (60) to N equations becomes significant if $\alpha_1 = O(N^3)$. In theory, accuracy is improved by increasing N and this is confirmed in figure

8. For $N = 20$ the difference between the results obtained using the mode-matching method and those given by the Wiener-Hopf method is minimal.

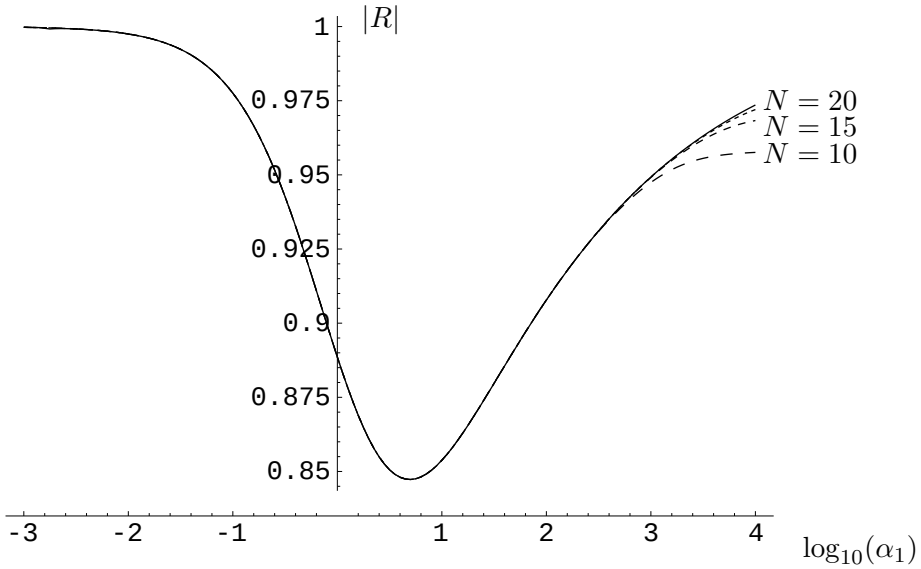

Figure 8: Comparison of the modulus of the reflected fluid-coupled structural mode against $\log_{10}(\alpha_1)$ for the Wiener-Hopf solution (solid line) and the membrane/membrane problem (dashed) truncated to N equations. Case (i) edge conditions are applied, and $a = b = 2.5$, $\mu_1 = 1.6$, $\mu_2 = 5$ and $\alpha_2 = 10$.

Figure 9 compares the reflection coefficient for varying α_2 when the edge conditions specified as case (iv) are applied. All other parameters are fixed, that is, $a = b = 2.5$, $\mu_1 = 1.6$, $\mu_2 = 5$ and $\alpha_1 = 10$. The same trends are observed regarding accuracy for the eigenfunction expansion method for

severe truncation.

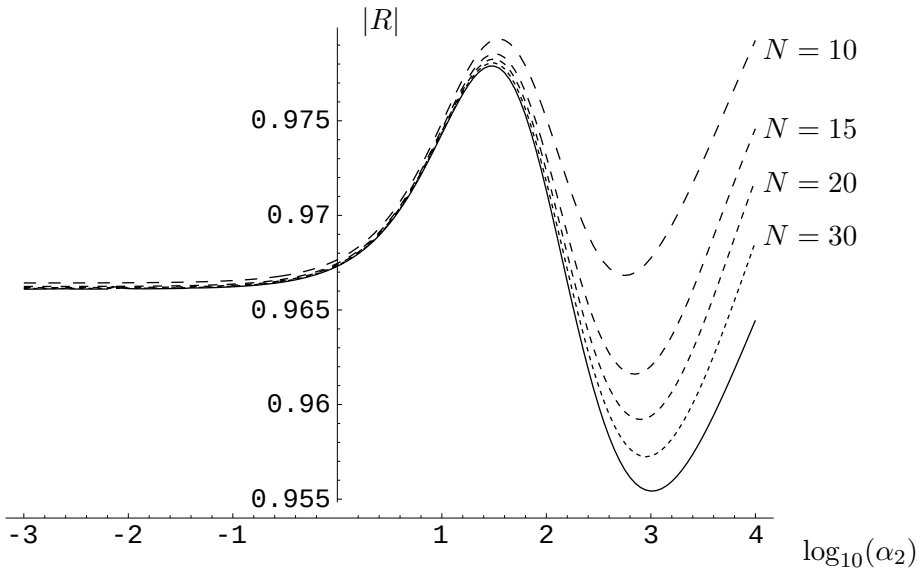

Figure 9: Comparison of the modulus of the reflected fluid-coupled structural mode against $\log_{10}\alpha_2$ for the Wiener-Hopf solution (solid line) and the membrane/membrane problem (dashed) truncated to N equations. Case (iv) edge conditions are applied, and $a = b = 2.5$, $\alpha_1 = 10$, $\mu_1 = 1.6$ and $\mu_2 = 5$.

The results discussed above are for the special case $a = b$, whereas the main purpose of this article is to investigate the general case $b > a$ for which there are no exact analytic results available against which to compare the results obtained using the mode-matching technique of §3.1. However, as mentioned in §2, it is possible to choose large and/or small values of the parameters α_j and μ_j, $j = 1, 2$ in order to establish limiting behaviours of the membrane surfaces. For example, setting $\alpha_2 >> 1$ with moderate μ_2 will force the right hand membrane to behave like a soft surface satisfying (approximately) the condition $\phi_2(x, b) = 0$, $x > 0$. Whereas, choosing $\alpha_1 << 1$ and $\mu_1 << 1$ causes $\eta_0 \to 1$ and $\eta_1 \to 0$ so that the structural wave reduces to a plane wave and the left hand membrane mimics a rigid surface, that is $\phi_y(x, a) = 0$, $x < 0$. (Note that, the choice of edge conditions is immaterial for these limiting cases.) With these restrictions on the parameters, the modulus of the reflection coefficient for $b > a$ can be compared both with the results for the hard/soft problem summarized in (4) – (6) and also with the large α results for the eigenfunction expansion problem presented

in §2.2. It is clear, from figure 10, that the level of agreement between the three solutions plotted is excellent. Note that, as in figures 4 – 6, the graph demonstrates the characteristic peaks every time b increases sufficiently to switch on a new transmitted mode.

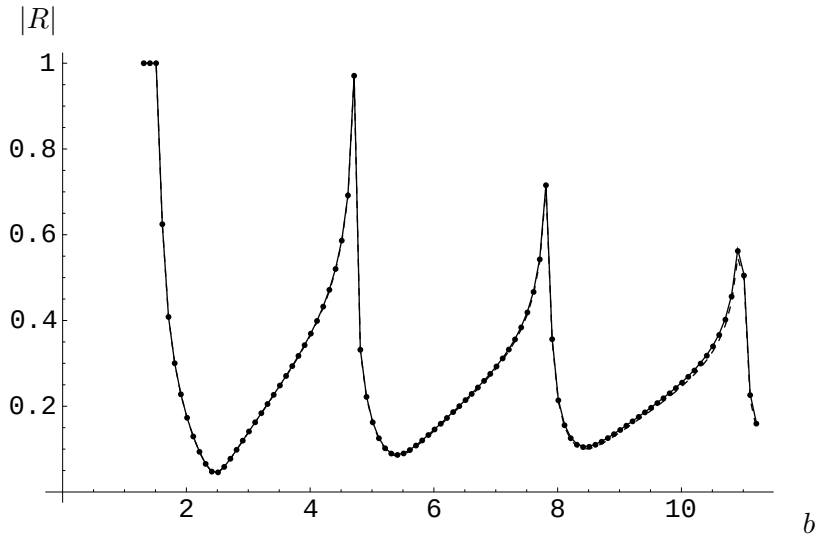

Figure 10: Comparison of the modulus of the reflection coefficient of the fundamental mode for the hard/soft problem (solid line), the heavy fluid-loading limiting case ($\alpha >> 1$) of the hard/membrane problem and the limiting case μ_1,$\alpha_1 << 1$ with $\alpha_2 >> 1$ of the membrane/membrane problem (dashed line), $a = 1.211$.

The next two graphs show the distribution of power between the two fluid regions and the two membranes. The power transmitted in the duct of height b is given by (A.105) and a minor modification to the notation gives the appropriate expression for the duct of height a. Hence, the power balance is given by

$$\begin{aligned} 1 \quad \equiv \quad & \frac{\alpha_1 \cosh^2(\tau_0 a)}{\eta_0 D_0} \Re \left\{ \sum_{n=0}^{\infty} |A_n|^2 \eta_n \left(\frac{a}{2} + \frac{\sinh(2\tau_n a)}{4\tau_n} \right) \right. \\ + \quad & \sum_{n=0}^{\infty} |B_n|^2 \nu_n \left(\frac{b}{2} + \frac{\sinh(2\gamma_n b)}{4\gamma_n} \right) + \sum_{n=0}^{\infty} \frac{|A|^2 \eta_n}{\alpha_1} \tau_n^2 \sinh^2(\tau_n a) \\ + \quad & \left. \sum_{n=0}^{\infty} \frac{|B|^2 \nu_n}{\alpha_2} \gamma_n^2 \sinh^2(\gamma_n b) \right\}. \end{aligned} \tag{70}$$

The first two quantities on the right hand side of (70) correspond to the reflected and transmitted power in the two separate fluid regions, whilst the third and forth terms are the power flux along the respective membranes. These four terms are plotted in figures 11 and 12 for case in which both membranes are of mass 2/3 kg per unit area but have different tensions. The tension (per metre in the z direction) for the left hand membrane is 4000/3 N whilst that for the right hand membrane is 8000/3 N. As in §2.2, the density of air is taken as 1.2043 kg m^{-3} and the sound speed in air as 343.5 ms^{-1}.

Figure 11 shows the distribution of power for forcing frequency of 100 Hz with the physical height of the left hand duct fixed at 0.5 m (thus, $a = 0.915$) as the height of the right hand duct varies from 0.5 to 6.5 m (thus, b varies from 0.915 to 11.9). The values of all other parameters are given in the caption. In marked contrast with figure 5 of §2.2, the power flux reflected along the left hand membrane dominates the power balance. This difference in behaviour is discussed in detail below. Note that, the values of b at which new right hand duct modes cut-on are clearly visible.

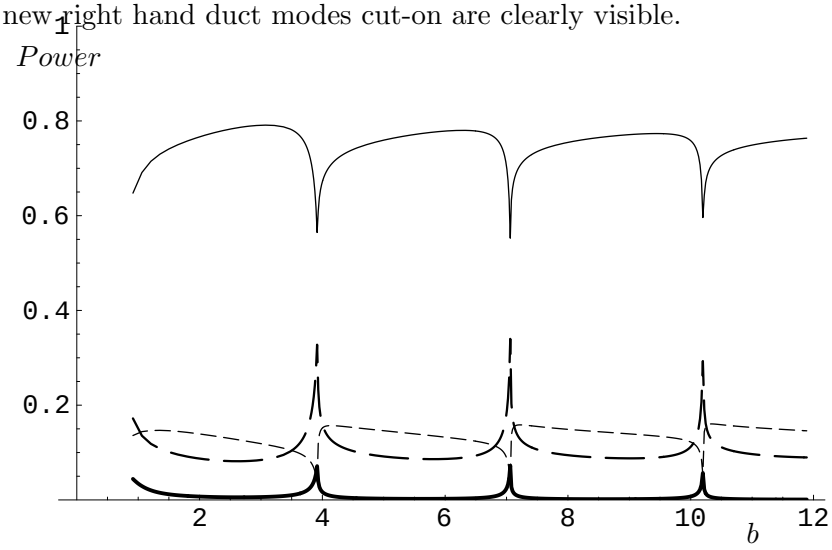

Figure 11: Distribution of power between the two fluid regions and the two membrane as right hand membrane bounded duct height varies: *thin solid line* ≡ left hand membrane; *thick solid line* ≡ right hand membrane; *long bold dash* ≡ reflected and *short dash* ≡ transmitted. (Frequency is 100 Hz and $a = 0.91$, $\alpha_1 = 58.26$, $\alpha_2 = 29.13$, $\mu_1 = 7.68$, $\mu_2 = 5.43$.)

Figure 12 shows the distribution of power for fixed geometry and membrane parameters as the forcing frequency increases from $5 - 650$ Hz. In this

case, the physical heights of the left and right hand ducts are 1.1 and 1.5 m respectively. Here again, most of the power is reflected along the left hand membrane which contrasts with figure 6 of §2.2. Indeed, for frequencies above 650 Hz in excess of 95% of the power is reflected in this manner. Although less clear than in figure 11, there are a number of peaks and troughs visible on all the lines in figure 12 and, as usual, these correspond to new modes being cut-on in either the left or right hand duct.

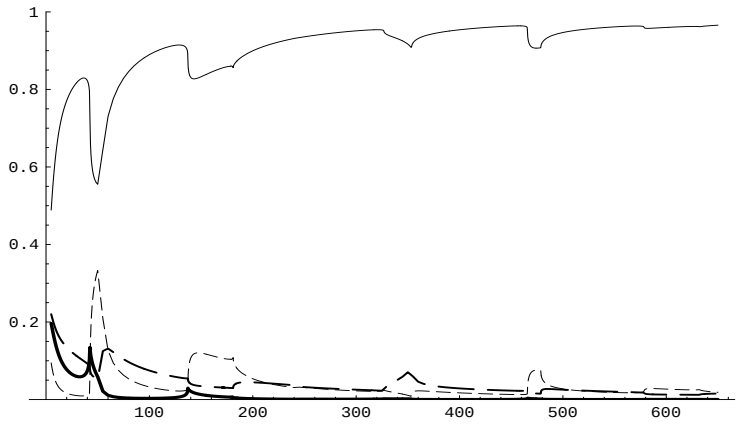

Figure 12: Distribution of power between the two fluid regions and the two membranes as frequncy varies: *thin solid line* ≡ left hand membrane; *thick solid line* ≡ right hand membrane; *long bold dash* ≡ reflected and *short dash* ≡ transmitted. (Here, $a/b = 11/15$, $\mu_1 = 7.68$ and $\mu_2 = 5.43$.)

The two problems, that is the hard/membrane problem of §2 and the membrane/membrane problem considered here, exhibit significantly different behaviours with regard to the distribution of power in the various fluid regions and membranes. The primary reason for this is the different forcing mechanisms and the low level of fluid-structure interaction. The true measure of fluid-loading is the quantity α/μ^2 which, from (A.78), is given by

$$\frac{\alpha}{\mu^2} = \frac{\rho}{\rho_m k}. \tag{71}$$

For the membrane mass and air density specified in this article, $\alpha/\mu^2 \approx 1$ when the frequency is 98 Hz. As frequency increases above this level, α/μ^2 steadily decreases indicating less and less fluid-structure interaction. In

consequence, for frequencies over 100 Hz, the power tends to remain in the medium in which it was introduced. For example, in the hard/membrane problem the forcing takes the form of a plane wave which propagates through the fluid. As frequency increases the fluid and membrane motions uncouple and the vast majority of the power is transmitted through the fluid region of the membrane bounded duct (see figure 6). Only at very low frequencies is a significant proportion of the power reflected along the rigid duct or transmitted in the membrane. In contrast the membrane/membrane problem is forced by a fluid coupled structural wave which propagates along the left hand membrane. In this case, as frequency increases and the fluid-structure interaction decreases, the left hand membrane behaves like a string vibrating *in vacuo*. Thus, the structural wave travels along the membrane and is reflected at the discontinuity with only a small loss in power (see figure 12).

4 Discussion

The problems discussed in this article demonstrate how a particular class of problem may be solved by utilizing the orthogonality relation appropriate to the eigen-problem obtained through separation of variables. The class of problem is vast, namely the reflection and transmission of plane or fluid-coupled structural waves at a discontinuity in height and/or material property in an otherwise infinite waveguide. It is well known that for cases where there is no change in height such problems can be solved using the Wiener-Hopf technique. However, it should be noted that the classical Wiener-Hopf technique is appropriate only for problems in which the planar boundaries are described by two-part conditions. The modified Wiener-Hopf technique can be applied to problems having three-part boundary conditions but the calculations are cumbersome and require either asymptotic interpretation or numerical evaluation of a pair of coupled integral equations (see, for example, [13]). Other extensions of the Wiener-Hopf technique deal with semi-infinite but non-planar geometries. In such cases, the Wiener-Hopf equation assumes a matrix form but exact factorization can be performed in only a small minority of cases and for the vast majority of problems an approximate factorization is necessary (see [14]). All such extensions to the Wiener-Hopf technique are inappropriate if the scattering structure has any vertical components and alternative approaches must then be employed as discussed in [15]. In contrast, the mode-matching method described here is not limited either to waveguides with planar boundaries or to two-part problems. In principle, the waveguide may undergo several changes in height

and material property and, provided the correct orthogonality relation is utilized in each duct region, the solution can still be obtained in a relatively straightforward manner.

The mode-matching method does, of course, have its limitations. The solution takes the form of an infinite system of algebraic equations which are difficult to interpret asymptotically and must, therefore, be solved numerically. Truncation or iteration are the usual methods by which infinite systems are solved but, in either case, it is necessary that the system converges adequately. It is known that in problems of this class the convergence of the infinite system is inversely proportional to the strength of the corner singularity of the fluid velocity potential (see [16]). Indeed, this is borne out by the hard/soft problem for which the system converged very slowly even after the leading order terms were subtracted out of the matrix. However, in the membrane/membrane problem the fluid velocity potential is not singular at either corner. This is reflected in the behaviour of the infinite system which, for moderate values of the parameters, gave highly accurate results even for radical truncation when as few as 12 equations were retained. The power plots of §2.2 and §2.3 were computed using this level of truncation and table 1 confirms this to be appropriate. A further limitation is the class of problems for which the method is appropriate. Although vast, it is characterized by the fact that the propagation medium is contained within the waveguide. The method cannot be applied to problems in which the walls are wave-bearing and there is fluid extending to infinity outside the duct boundaries. For problems of this type the eigenfunctions are not complete, as is evident by the fact that there is always a branch-cut contribution to the far-field even within the duct itself.

Finally, it is a feature of many numerical mode-matching schemes that they automatically conserve power (see [17]). This is indeed true for the power balances presented in §2 and §3 of this article and a brief proof is presented below for the latter case. It will be assumed that M_1 and M_2 real modes propagate in the left and right hand ducts respectively, and that the system of equations (60) is truncated to N equations where $N > M_1$ and $N > M_2$. Then (70) may be written as

$$\frac{\eta_0 D_0}{\alpha_1 \cosh^2(\tau_0 a)} = \Re\left\{\sum_{n=0}^{N} A_n^* \left(A_n \eta_n \frac{D_n}{\alpha_1}\right) + \sum_{n=0}^{N} B_n^* \left(B_n \nu_n \frac{C_n}{\alpha_2}\right)\right\}. \qquad (72)$$

where the superscript * indicates the complex conjugate. Here the terms representing power flow through the fluid and that transmitted along the membrane have been combined and expressed in terms of the quantities D_n

(for the left hand duct) and C_n (for the right hand duct) which are defined in (A.96). It is a straightforward procedure to use the truncated forms of (60) and (53) to replace the quantities $A_n\eta_n D_n/\alpha_1$ and $B_n\nu_n C_n/\alpha_2$ which are bracketed in (72). Thus,

$$\begin{aligned}\Re\left\{\sum_{n=0}^{N} A_n^* A_n \eta_n \frac{D_n}{\alpha_1} \right. &+ \left. \sum_{n=0}^{N} B_n^* B_n \nu_n \frac{C_n}{\alpha_2}\right\} = \Re\left\{\sum_{n=0}^{N} A_n^* \eta_n \sum_{m=0}^{N} B_m T_{nm}\right. \\ &+ \frac{F}{\alpha_1}\sum_{n=0}^{N} A_n^*\eta_n\tau_n \sinh(\tau_n a) - \frac{A_0^*\eta_0 D_0}{\alpha_1\cosh(\tau_0 a)} \\ &- \frac{iE}{\alpha_2}\sum_{n=0}^{N} B_n^*\gamma_n\sinh(\gamma_n b) + \frac{2\eta_0}{\cosh(\tau_0 a)}\sum_{n=0}^{N} B_n^* T_{0n} \\ &- F\sum_{\ell=0}^{N}\sum_{n=0}^{N} B_n^* \frac{T_{\ell n}\eta_\ell\tau_\ell\sinh(\tau_\ell a)}{D_\ell} \\ &- \left.\left.\alpha_1\sum_{\ell=0}^{N}\sum_{m=0}^{N} B_m \frac{T_{\ell m}\eta_\ell}{D_\ell}\left(\sum_{n=0}^{N} B_n^* T_{\ell n}\right)\right\}\right. \end{aligned} \tag{73}$$

The quantity in parentheses which appears in the last term of (73) can be replaced using the complex conjugate of (53). (The reader is reminded that the quantities $\tau_\ell \sinh(\tau_\ell a)$ and $T_{\ell n}$ are real for all $\ell = 0, 1, 2, \ldots$, $n = 0, 1, 2, \ldots$.) Hence, after some rearrangement, it is found that

$$\begin{aligned}\Re\left\{\sum_{n=0}^{N} A_n^* A_n \eta_n \frac{D_n}{\alpha_1} \right. &+ \left. \sum_{n=0}^{N} B_n^* B_n \nu_n \frac{C_n}{\alpha_2}\right\} = \Re\left\{\frac{D_0\eta_0}{\alpha_1\cosh^2(\tau_0 a)}\right. \\ &+ \frac{F}{\alpha_1}\left(\sum_{n=0}^{N} A_n^*\eta_n\tau_n\sinh(\tau_n a) - \frac{\eta_0\tau_0\sinh(\tau_0 a)}{\cosh(\tau_0 a)}\right) \\ &- \frac{iE}{\alpha_2}\sum_{n=0}^{N} B_n^*\gamma_n\sinh(\gamma_n b) \\ &+ 2i\Im\left\{F^*\sum_{\ell=0}^{N}\sum_{m=0}^{N} B_m T_{\ell m}\frac{\eta_\ell\tau\ell\sinh(\tau_\ell a)}{D_\ell}\right\} \\ &+ \left.\left.\frac{4i\eta_0}{\cosh(\tau_0 a)}\Im\left\{\sum_{n=0}^{N} B_n^* T_{0n}\right\}\right\}\right. \end{aligned} \tag{74}$$

The edge conditions for the truncated form of the membrane/membrane problem dictate that the second and third terms on the right hand side of

(74) vanish, and clearly the two imaginary components do not contribute. Thus, the first term of (74) confirms the power balance of (72).

The above result in fact holds true for any $N > 0$. It is remarkable that (72) appears always to hold *even* when $N < M_2$. Table 1 demonstrates this: here R is the power reflected in the fluid and ML is the power travelling along the membrane of the left hand duct, whilst T is the power transmitted in the fluid and MR is the power propagating along the membrane of the right hand duct. Clearly, (72) is satisified for $N = 2$ even though $M_2 = 3$.

N	2	3	7	12	32	52
R	0.05918	0.04250	0.04888	0.04960	0.04986	0.04993
ML	0.79941	0.57402	0.66021	0.66991	0.67345	0.67438
T	0.14055	0.37193	0.28176	0.27148	0.26781	0.26684
MR	0.00086	0.01155	0.00916	0.00901	0.00888	0.00885
Total	1.	1.	1.	1.	1.	1.

Table 1: The power balance for different values of N: $a = 0.27$, $b = 4.11$, $\mu_1 = 5.43$, $\alpha_1 = 19.42$, $\mu_2 = 7.68$ and $\alpha_2 = 38.84$.

It can be concluded that equation (72) is an algebraic identity which happens to coincide with the power balance if and only if $N \geq M_1$, $N \geq M_2$ *and* N is sufficiently large for the solution of the truncated system of equations to have converged to the solution of the physical problem. The power balance must hence be viewed as a means of validating the algebraic integrity of the code and not as a means of testing whether its results represent the solution of the physical problem in mind.

A Appendix

A.1 The orthogonality relation

The orthogonality relation used in §2 and §3 of this article is derived here using the appropriate unforced, non-dimensional boundary value problem. Thus, the governing equation is

$$\nabla^2\phi + \phi = 0, \qquad 0 \leq y \leq b, \quad -\infty < x < \infty. \tag{A.75}$$

and the condition at the rigid surface is

$$\frac{\partial\phi}{\partial y} = 0, \qquad y = 0. \tag{A.76}$$

The membrane boundary condition is given by

$$\left\{\frac{\partial^2}{\partial x^2}+\mu^2\right\}\phi_y+\alpha\phi=0, \qquad y=b, \tag{A.77}$$

where the non-dimensional fluid-loading parameter α and membrane wave number μ are defined by

$$\alpha=\frac{\omega^2\rho}{Tk^3} \qquad \text{and} \qquad \mu=\frac{c}{c_m}. \tag{A.78}$$

Here T is the membrane tension per unit length (in the z direction) , ρ is the the fluid density, ω is the radian frequency of the time harmonic disturbances, c is the fluid sound speed and $c_m=\sqrt{T/\rho_m}$ is the *in vacuo* speed of waves on the membrane (where ρ_m is the membrane mass per unit area).

Separable solutions to (A.75) that satisfy boundary conditions (A.76) and (A.77) have the form

$$\phi=\sum_{n=0}^{\infty}\sigma_n Y_n(y)e^{i\nu_n x}, \tag{A.79}$$

where the (complex) coefficients σ_n, $n=1,2,3,\ldots$ are arbitrary since the boundary value problem is unforced. The eigenfunctions, $Y_n(y), n=0,1,2,\ldots$, satisfy the system

$$\begin{aligned} Y_n^{''}(y)-\gamma_n^2 Y_n(y) &= 0, & \text{(A.80)}\\ (\gamma_n^2+1-\mu^2)Y_n^{'}(b)-\alpha Y_n(b) &= 0, & \text{(A.81)}\\ Y_n^{'}(0) &= 0, & \text{(A.82)} \end{aligned}$$

with $\gamma_n=(\nu_n^2-1)^{\frac{1}{2}}$. Here the prime indicates differentiation with respect to y. To obtain the orthogonality relation, note that (A.81) and (A.82) can be combined as

$$\Big[(\gamma_n^2-\gamma_m^2)Y_n^{'}(y)Y_m^{'}(y)-\alpha(Y_n(y)Y_m^{'}(y)-Y_m(y)Y_n^{'}(y))\Big]_0^b=0. \tag{A.83}$$

Equation (A.83) is easily recognised to have the integral form

$$(\gamma_n^2-\gamma_m^2)\int_0^b\frac{d}{dy}\{Y_n^{'}(y)Y_m^{'}(y)\}\,dy-\alpha\int_0^b\{Y_n(y)Y_m^{''}(y)-Y_m(y)Y_n^{''}(y)\}\,dy=0. \tag{A.84}$$

On integrating the first term of (A.84) and rearranging the second using (A.80), it is found that

$$(\gamma_n^2 - \gamma_m^2)\left\{Y_n'(b)Y_m'(b) + \alpha\int_0^b Y_n(y)Y_m(y)\,dy = 0\right\}. \tag{A.85}$$

It follows that,

$$\alpha\int_0^b Y_n(y)Y_m(y)\,dy + Y_n'(b)Y_m'(b) = 0, \quad m \neq n. \tag{A.86}$$

To evaluate the left hand side of (A.86) for $m = n$ is a straightforward procedure since, from (A.80) – (A.82), $Y_n(y) \equiv \cosh(\gamma_n y)$. It follows that the orthogonality relation for the eigen-problem specified by (A.80)–(A.82) is

$$\alpha\int_0^b Y_m(y)Y_n(y)dy + Y_m^{'}(b)Y_n^{'}(b) = \delta_{mn}C_n \tag{A.87}$$

where

$$C_n = \frac{Y_n'(b)}{2\gamma_n}\frac{d}{d\gamma}K(s,b)\rfloor_{\gamma=\gamma_n} \tag{A.88}$$

and δ_{mn} is the Kronecker delta. Note that $K(s,b)$ is the despersion function, see (18) and is consistent with (A.81) which states that $K(\nu_n, b) = 0$.

The orthogonality relation, (A.87), can be expressed as an inner product of eigenfunctions

$$(Y_m, Y_n) = \delta_{mn}C_n. \tag{A.89}$$

This definition may be extended to functions that are sufficiently differentiable over the interval $0 \leq y \leq b$ and have the form

$$g(y) = \sum_{m=0}^{\infty} B_m Y_m(y) \tag{A.90}$$

to obtain

$$(g, Y_n) = \alpha\int_0^b g(y)Y_n(y)\,dy + g'(b)Y_n'(b) = B_nC_n. \tag{A.91}$$

This definition makes application of the orthogonality relation a simple procedure as was demonstrated in §2 and §3.

A.2 Derivation of supplementary identities

The problem discussed in §3 of this article comprises two semi-infinite sections of duct of different heights, both bounded by membranes. The reader is refered to §3 for details but is reminded that the membranes have different material properties. Appropriate forms of the orthogonality relation derived above are used to match the normal velocity and pressure at the vertical interface between the two duct sections. The resulting system of equations contains the kernel $T_{\ell m}$ (see (54)) which is given by

$$T_{\ell m} = \frac{\tau_\ell \sinh(\tau_\ell a)\cosh(\gamma_m a) - \gamma_m \sinh(\gamma_m a)\cosh(\tau_\ell a)}{\tau_\ell^2 - \gamma_m^2}. \tag{A.92}$$

The following identities can be proven in a straightforward manner using contour integration

$$\alpha_1 \sum_{\ell=0}^{\infty} \frac{T_{\ell m}}{D_\ell} = \alpha_2 \sum_{m=0}^{\infty} \frac{T_{\ell m}}{C_m} \equiv 1, \tag{A.93}$$

$$\sum_{\ell=0}^{\infty} \frac{\tau_\ell^2 \sinh^2(\tau_\ell a)}{D_\ell} = \sum_{m=0}^{\infty} \frac{\gamma_m^2 \sinh^2(\gamma_m b)}{C_m} \equiv 1, \tag{A.94}$$

and

$$\sum_{\ell=0}^{\infty} \frac{\tau_\ell \sinh(\tau_\ell a) T_{\ell m}}{D_\ell} = \sum_{m=0}^{\infty} \frac{\gamma_m \sinh(\gamma_m a) T_{\ell m}}{C_m} \equiv 0 \tag{A.95}$$

where

$$C_m = \frac{\gamma_m \sinh(\gamma_m b)}{2\nu_m} K_2'(s,b)\rfloor_{s=\nu_n} \quad \text{and} \quad D_\ell = \frac{\tau_\ell \sinh(\tau_\ell a)}{2\eta_\ell} K_1'(s,a)\rfloor_{s=\eta_\ell}. \tag{A.96}$$

Note that the prime indicates differentiation with respect to s. The derivation of the right-hand sum of (A.93) will be outlined briefly. Consider the contour integral, I, given by

$$I = \frac{1}{2\pi i} \oint_\Gamma \frac{s}{K_2(s,b)} \frac{\tau_\ell \sinh(\tau_\ell a)\cosh(\gamma a) - \gamma \sinh(\gamma a)\cosh(\tau_\ell a)}{(\tau_\ell^2 - \gamma^2)\gamma \sinh(\gamma b)}\, ds. \tag{A.97}$$

Here $\gamma = (s^2-1)^{1/2}$ and $\tau_\ell = (\nu_\ell^2 - 1)^{1/2}$ where ν_ℓ is any root of $K_1(s,a)$. The path of integration, Γ, is D shaped lying along the real axis (indented above any poles on the negative side and below any on the positive side) from $-R$ to R, where $R \gg 1$, and then following a semi-circular arc in the

upper half of the complex plane from R back to $-R$. Clearly there are two families of simple poles within the contour Γ and it follows that

$$\begin{aligned} I &= \sum_{m=0}^{M} \frac{\nu_m T_{\ell m}}{K'(\nu_m, b)\gamma_m \sinh(\gamma_m b)} \\ &- \frac{1}{b\alpha_2} \sum_{j=0}^{J} \frac{\tau_\ell \sinh(\tau_\ell a)\cos(j\pi a/b) + (j\pi/b)\sin(j\pi a/b)\cosh(\tau_\ell a)}{\epsilon_j(\tau_\ell^2 + (j\pi/b)^2)} \end{aligned} \tag{A.98}$$

where M and J are the number of poles of each family within the contour and $\epsilon_0 = 2$ whilst $\epsilon_j = 1$, $j = 1, 2, \ldots$. Now, as $R \to \infty$, the integral along the real axis is zero (since the integrand is an odd function of s) and the contribution from the arc at infinity tends to zero. Hence, on using (A.96)

$$\begin{aligned} \sum_{m=0}^{\infty} \frac{T_{\ell m}}{C_m} &= \frac{2}{b\alpha_2} \left(\tau_\ell \sinh(\tau_\ell a) \sum_{j=0}^{\infty} \frac{\cos(j\pi a/b)}{\epsilon_j(\tau_\ell^2 + (j\pi/b)^2)} \right. \\ &\left. + \cosh(\tau_\ell a) \sum_{j=0}^{\infty} \frac{(j\pi/b)\sin(j\pi a/b)}{\epsilon_j(\tau_\ell^2 + (j\pi/b)^2)} \right). \end{aligned} \tag{A.99}$$

The sums on the right hand side of (A.99) can be evaluated exactly (see [18, p. 47], and it is found that

$$\sum_{m=0}^{\infty} \frac{T_{\ell m}}{C_m} = \frac{1}{\alpha_2}. \tag{A.100}$$

All the other sums listed above can be evaluated in an analogous manner.

A.3 Transmission of power along a membrane bounded duct

The power transmitted along a duct of height b with membrane walls (such as that on the right hand side of the problem considered in §3 of this paper) comprises two components: that transmitted through the fluid and the flux in the membrane. For the fluid region the rate of change of energy across an arbitrary surface, S, is

$$\frac{\partial E}{\partial t}\rfloor_{fluid} = \Re\{ \int_S PV^* \, ds\} \tag{A.101}$$

where P is the fluid pressure and V the normal component of velocity. Given that the surface, S, occupies the region $0 \le y \le b$, $0 \le z \le 1$, $x = x_0$ where

x_0 is arbitrary, then, in terms of the non-dimesional, time harmonic fluid velocity potential, this is

$$\frac{\partial E}{\partial t}\rfloor_{fluid} = \frac{\rho\omega^3}{k^5}\,\Re\left\{i\int_0^b \phi\left(\frac{\partial\phi}{\partial x}\right)^*\,dy\right\} \tag{A.102}$$

where the integration with respect to z has been performed. The power flux along the membrane per unit length in the z direction is given by

$$\frac{\partial E}{\partial t}\rfloor_{memb} = T_2\,\Re\left\{\frac{\partial w}{\partial t}\left(\frac{\partial w}{\partial x}\right)^*\right\} \tag{A.103}$$

where (using the appropriate notation for the right hand membrane of §3) T_2 is the membrane tension per unit length in the z direction and w is the membrane displacement. Again, this can be expressed in terms of the non-dimensional fluid velocity potential as

$$\frac{\partial E}{\partial t}\rfloor_{memb} = \frac{\rho\omega^3}{k^5}\frac{1}{\alpha_2}\,\Re\left\{i\frac{\partial\phi}{\partial y}\left(\frac{\partial^2\phi}{\partial y\partial x}\right)^*\right\}. \tag{A.104}$$

Thus, on substituting the eigen-expansion (46) for the fluid velocity potential into (A.102) and (A.104), it is found that

$$\begin{aligned}\frac{\partial E}{\partial t}\rfloor_{total} \;=\; \frac{\rho\omega^3}{k^5}\,\Re\Bigg\{&\sum_{n=0}^{\infty}|B_n|^2\nu_n\left(\frac{b}{2}+\frac{\sinh(2\gamma_n b)}{4\gamma_n}\right)\\ &+\sum_{n=0}^{\infty}\frac{|B_n|^2}{\alpha_2}\nu_n\gamma_n^2\sinh^2(\gamma_n b)\Bigg\}.\end{aligned} \tag{A.105}$$

Here the first term is the power flow through the fluid and the second term corresponds to the membrane flux. Note that the cross-terms (i.e. terms containing B_mB_n where $m\neq n$) cancel out between the two contributions. In order to view the two components of the power separately (A.105) is used in §2 and §3 of this paper. It is, however, a straightforward procedure to combine both quantities and express the power flow in terms of the quantity C_n, see (72).

Acknowledgement

D. P. Warren gratefully acknowledges the financial support provided by the Department of Mathematical Sciences, Brunel University, U.K. during the time this work was carried out.

References

[1] Keller, J. B. "Geometric theory of diffraction" *J. Optic. Soc. Am.* **52**, 116–130 (1962).

[2] Cannell, P. A. "Edge scattering of aerodynamic sound by a lightly loaded elastic half-plane" *Proc. R. Soc. Lond. A* **347**, 213–238 (1975).

[3] Brazier-Smith, P. R. "The acoustic properties of two co-planar half-plane plates" *Proc. R. Soc. Lond. A* **409**, 115–139 (1987).

[4] Norris, A.N. and Wickham, G.R. "Acoustic diffraction from the junction of two flat plates" *Proc. R. Soc. Lond. A* **451**, 631–655 (1995).

[5] Roseau, M. *Asymptotic Wave Theory*, North-Holland, Amsterdam (1976).

[6] Evans, D.V. "A solution of a class of boundary value problems with smoothly-varying boundary conditions" *Q. Jl Mech appl. Math.* **38**, 521–536 (1985).

[7] Fernyhough, M. and Evans, D.V. "Comparison of a step approximation to an exact solution of acoustic scattering in a uniform-width pipe with nonuniform wall impedance" *Q. Jl Mech appl. Math.* **49**, 419–437 (1996).

[8] Grant, A.D. and Lawrie, J.B. "Acoustic scattering in a duct with elastic plate walls having continuously varying bending characteristics" *Q. Jl Mech appl. Math.* **53**,299–321 (2000).

[9] Warren, D.P. *Thesis, Brunel University, UK.* (1999)

[10] Peat, K.S. "The acoustical impedance at the junction of an extended inlet or outlet duct" *J Sound Vib* **150**, 101-110 (1991).

[11] Dalrymple, R.A. and Martin, P.A. "Water waves incident on an infinitely long rectangular inlet" *Appl. Ocean Res.* **18**, 1–11 (1996).

[12] Lawrie, J.B. and Abrahams, I.D. "An orthogonality condition for a class of problem with high order boundary conditions; applications in sound/structure interaction" *Q. Jl Mech appl. Math.* **52**, 161–181 (1999).

[13] Lawrie, J.B. "Axisymmetric radiation from a finite gap in an infinite, rigid, circular duct" *I.M.A. J. Appl. Math.* **41**, 113–128 (1988).

[14] Lawrie, J.B. and Abrahams, I.D. "Acoustic radiation from two opposed, semi-infinite, co-axial cylindrical waveguides, Part II: separated edges" *Wave Motion* **19**, 83–109 (1994).

[15] Jones, D.S. "Diffraction by a thick semi-infinite plate" *Proc. R. Soc. Lond. A* **247**, 153–175 (1953).

[16] Evans, D.V. and Porter, R. "Hydrodynamic characteristics of an oscillating water column device" *Appl. Ocean Res.* **17**, 155-164 (1995).

[17] Kriegsmann, G. A. "The flanged waveguide antenna: Discrete reciprocity and conservation" *Wave motion* **29**, 81–95 (1999).

[18] Gradshteyn, I.S. and Ryzhik, I.M. Table of integrals, series and products. *Fifth Edition.* Academic Press (1994).